

Picornavirus Genome Replication

IDENTIFICATION OF THE SURFACE OF THE POLIOVIRUS (PV) 3C DIMER THAT INTERACTS WITH PV 3Dpol DURING VPg URIDYLYLATION AND CONSTRUCTION OF A STRUCTURAL MODEL FOR THE PV 3C₂-3Dpol COMPLEX*

Received for publication, September 20, 2007, and in revised form, November 8, 2007. Published, JBC Papers in Press, November 9, 2007, DOI 10.1074/jbc.M707907200

Miaoqing Shen^{1,2}, Zachary J. Reitman^{1,3}, Yan Zhao, Ibrahim Moustafa, Qixin Wang, Jamie J. Arnold, Harsh B. Pathak⁴, and Craig E. Cameron⁵

From the Department of Biochemistry and Molecular Biology, Pennsylvania State University, University Park, Pennsylvania 16802

Picornaviruses have a peptide termed VPg covalently linked to the 5'-end of the genome. Attachment of VPg to the genome occurs in at least two steps. First, Tyr-3 of VPg, or some precursor thereof, is used as a primer by the viral RNA-dependent RNA polymerase, 3Dpol, to produce VPg-pUpU. Second, VPg-pUpU is used as a primer to produce full-length genomic RNA. Production of VPg-pUpU is templated by a single adenylate residue located in the loop of an RNA stem-loop structure termed oril by using a slide-back mechanism. Recruitment of 3Dpol to and its stability on oril have been suggested to require an interaction between the back of the thumb subdomain of 3Dpol and an undefined region of the 3C domain of viral protein 3CD. We have performed surface acidic-to-alanine-scanning mutagenesis of 3C to identify the surface of 3C with which 3Dpol interacts. This analysis identified numerous viable poliovirus mutants with reduced growth kinetics that correlated to reduced kinetics of RNA synthesis that was attributable to a change in VPg-pUpU production. Importantly, these 3C derivatives were all capable of binding to oril as well as wild-type 3C. Synthetic lethality was observed for these mutants when placed in the context of a poliovirus mutant containing 3Dpol-R455A, a residue on the back of the thumb required for VPg uridylylation. These data were used to guide molecular docking of the structures for a poliovirus 3C dimer and 3Dpol, leading to a structural model for the 3C₂-3Dpol complex that extrapolates well to all picornaviruses.

Picornavirus and picorna-like viruses cause diseases in humans, animals, insects, and plants (1, 2). The genome of these

viruses is a single-stranded RNA of positive polarity that is, on average, 7500 nucleotides in length and that contains a protein, VPg (virion protein genome-linked), covalently attached to its 5'-end (1, 2). Picornavirus negative-strand RNA also contains VPg covalently attached to its 5'-end (1, 2). The role(s) of VPg in the metabolism of the viral genomic and antigenomic RNA is not known but could prevent recognition by the innate immune system, enhance RNA stability, and/or contribute to efficient packaging of the viral genome.

Attachment of VPg to the 5'-end of picornaviral RNAs is, minimally, a two-step process. Tyr-3 of VPg, or some precursor thereof, is used as a primer by the viral RNA-dependent RNA polymerase, 3Dpol, to produce VPg-pUpU, which in turn serves as a primer for production of full-length genomic and antigenomic RNAs (3). To date, two templates for 3Dpol-catalyzed uridylylation of VPg have been discovered as follows: the poly(rA) tail located on the 3'-ends of all picornaviral genomic RNAs (4); an RNA stem-loop most often located in protein-coding sequence of picornaviral genomic RNA that has been termed the cre (cis-acting replication element) or oril (origin of replication internal) (5, 6). There is currently some debate regarding the use of one or both of these elements for VPg uridylylation. Some studies suggest that the poly(rA) tail is the template for production of VPg-pUpU employed for antigenomic RNA synthesis, and oril is the template for production of VPg-pUpU employed for genomic RNA synthesis (7–9). Other studies suggest that oril is the template for production of VPg-pUpU employed for both antigenomic and genomic RNA syntheses (10). Despite this controversy, it is clear that oril-templated production of VPg-pUpU is an essential reaction for picornavirus genome replication.

Oril-templated production of VPg-pUpU has been reconstituted *in vitro* from purified components for a variety of picornaviruses (5, 10–14). Importantly, these *in vitro* systems explain and predict phenotypes observed biologically (5, 10–14). The minimal requirements for efficient VPg uridylylation *in vitro* are as follows: oril, 3Dpol, VPg peptide, 3C(D) protein, and UTP (5). Oril varies in length between picornaviruses, but all can be described as having a loop and a stem. The stem can be divided into two parts: upper stem and lower stem (3). The loop and upper stem are both necessary and sufficient for efficient VPg uridylylation (3). Picornaviral 3CD protein is a fusion between 3C protease and 3D polymerase domains. Protein 3CD exhibits protease activity with a specificity and cata-

* This work was supported in part by NIAID Research Grant AI053531 from the National Institutes of Health (to C. E. C.). The costs of publication of this article were defrayed in part by the payment of page charges. This article must therefore be hereby marked "advertisement" in accordance with 18 U.S.C. Section 1734 solely to indicate this fact.

¹ Both authors contributed equally to this work.

² Present address: Dept. of Biomedical Sciences, Cornell University, Ithaca, NY 14853.

³ Recipient of a Department of Homeland Security scholarship. Present address: Medical Scientist Training Program, Duke University School of Medicine, Durham, NC 27705.

⁴ Present address: Dept. of Medical Oncology, Fox Chase Cancer Center, Philadelphia, PA 19111.

⁵ Recipient of Established Investigator Award 0340028N from the American Heart Association. To whom correspondence should be addressed: Dept. of Biochemistry and Molecular Biology, Pennsylvania State University, 201 Althouse Laboratory, University Park, PA 16802. Tel.: 814-863-8705; Fax: 814-865-7927; E-mail: cec9@psu.edu.

PV 3C Residues Required for VPg Uridylation

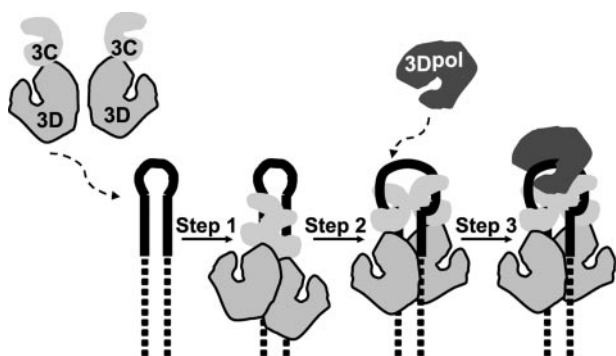


FIGURE 1. Assembly and organization of the picornavirus VPg ribonucleoprotein complex. Step 1, two 3C(D) molecules bind to oriI with the 3C domains contacting the upper stem (solid lines) and the 3D domains contacting the lower stem (dashed lines). Step 2, 3C dimer opens the RNA stem by forming a more stable interaction with single strands forming the stem. Step 3, 3Dpol is recruited to and retained in this complex by a physical interaction between the back of the thumb subdomain of 3Dpol and a surface of one or both 3C subunits of the dimer. Taken from Ref. 13.

lytic efficiency that is different from 3C but lacks polymerase activity, although the overall fold of the 3D domain of 3CD is quite similar to that of 3Dpol (15, 16). In addition to protease activity, the 3C domain alone and in the context of 3CD exhibits both specific and nonspecific RNA binding activity (12, 13, 17–34).

Our current model for assembly and organization of the picornavirus VPg uridylation complex is shown in Fig. 1. A dimer of 3C(D) binds to oriI with 3C domains interacting with the upper stem of oriI (Fig. 1, step 1) (13, 14). This complex isomerizes to unwind the stem such that each of the 3C domains interacts with a strand of the stem in a sequence-specific fashion, and the 3D domains interact with the lower stem (Fig. 1, step 2) (13, 14). Information on the interaction between the 3D domain and the lower stem is not currently available. Opening of the upper stem of oriI by 3C(D) has been suggested to organize the loop into a conformation that should be readily accommodated by 3Dpol (13, 36).⁶ 3Dpol is thought to be recruited to this complex and retained therein by an interaction between the back of the thumb subdomain of 3Dpol and an undefined surface of the 3C(D) dimer (Fig. 1, step 3) (13, 14). VPg or some precursor thereof joins the complex either along with (37, 38) or after 3Dpol (39). Finally, two rounds of UMP incorporation occur without dissociation of the peptide primer. Both uridylate residues are templated by a single adenylate residue by using a slide-back mechanism (40).

Molecular genetic, biological, biochemical, and physical data support the existence of an interaction between 3Dpol and the 3C(D) dimer that is required for picornavirus VPg uridylation (13, 14, 41). However, the specific surface(s) of 3C that interact with 3Dpol is unknown. We have used a reverse-genetic approach to identify residues of poliovirus (PV)⁷ 3C that interact with 3Dpol to facilitate formation and/or stabilization of the

VPg uridylation complex. We have identified numerous residues of 3C that localize to a single surface of the 3C dimer that influences VPg uridylation efficiency *in vitro* and RNA replication and virus production in cell culture. Importantly, only viable PV 3C mutants with slow growth phenotypes attributable to VPg uridylation defects unrelated to oriI binding exhibited synthetic lethality with a PV 3Dpol mutant that is known to be impaired for VPg uridylation *in vitro* (38). A structural model for the PV 3C₂-3Dpol complex was constructed by using a docking algorithm that is consistent not only with all of the new data on 3C reported here but also with all of the data on 3Dpol published previously by us (13, 14, 41) and others (32, 42, 43). This model extrapolates well to other members of the picornavirus family, thus providing a high resolution perspective of the picornavirus VPg uridylation complex. The impact of this model on our understanding of the structure, function, mechanism, and evolution of picornavirus VPg uridylation complexes and components thereof is discussed.

EXPERIMENTAL PROCEDURES

Materials—DNA oligonucleotides were from Integrated DNA Technologies, Inc.; Deep Vent DNA polymerase and restriction enzymes were from New England Biolabs; shrimp alkaline phosphatase was from U. S. Biochemical Corp.; T4 DNA ligase was from Invitrogen; Difco-NZCYM was from BD Biosciences; QIAEX beads were from Qiagen; RNase A was from Sigma; Ultrapure UTP solution was from GE Healthcare; [α -³²P]UTP (6000 Ci/mmol) was from Perkin-Elmer Life Sciences; synthetic PV VPg peptide was purchased from Alpha Diagnostic International (San Antonio, Texas); HeLa S3 cells were obtained from American Type Culture Collection and grown in DMEM/F-12 medium with 10% fetal bovine serum (Invitrogen) with 100 units/ml penicillin and 100 units/ml streptomycin; 3'-fluorescein-labeled oriI (29 nucleotides) was from Dharmacon, Inc.; and all other reagents and apparatuses were available through Fisher, VWR, or as indicated.

Construction of Mutated Viral cDNA Clones and Replicons—A SacII site and HpaI site were introduced in the PV open reading frame of pMoRA at positions 4498 and 5207, respectively, by using overlap-extension PCR with the viral cDNA (pMoRA, also known as pXpA-rib+ polyAlong) and replicon (pRLucRA, also known as pRLuc-rib+ polyAlong) (44) as template. Two PCR fragments were amplified using oligonucleotides 1–4 (Table 1), and these two fragments were then used as templates for amplification of a new fragment using oligonucleotides 1 and 2 (Table 1). The PCR product with the HpaI site was cloned into the pMoRA plasmid using SnaBI and BglII sites to yield pMoRA-HpaI. Introduction of HpaI into pRLucRA was performed as described above except using SpeI and BglII sites (oligonucleotide 5 in Table 1). Oligonucleotides 6–9 (Table 1) were used to amplify fragments with a SacII site. The PCR product was cloned into pUC18-3CD-BglII-EcoRI (45) to yield pUC18-3CD-BglII-SacII-EcoRI using BglII and AflIII sites. The fragment with the SacII site in pUC18-3CD-BglII-SacII-EcoRI was cloned into the pMoRA-HpaI and pRLuc-HpaI using BglII and EcoRI or BglII and ApaI, respectively, to yield pMoRA-HpaI-SacII and pRLuc-HpaI-SacII.

⁶ C. D. Amero, J. J. Arnold, I. M. Moustafa, C. E. Cameron, and M. P. Foster, submitted for publication.

⁷ The abbreviations used are: PV, poliovirus; WT, wild type; Tricine, N-[2-hydroxy-1,1-bis(hydroxymethyl)ethyl]glycine; PBS, phosphate-buffered saline; DMEM, Dulbecco's modified Eagle's medium; WT, wild type.

TABLE 1

Oligonucleotides used in this study

Restriction sites are bold; nucleotide changes are lowercase.

No.	Name	Sequence
1	pMo-SnaBI-F	5'-TTA TGT ACG TAC CAC CAG GAG CTC CAG TGC CCG AG -3'
2	pMo-BglII-R	5'-CGC AGA TCT CCA CTT CTT TGC CA -3'
3	PV-sil-HpaI-F	5'-GAA GGG TTG GAT AGT taa CAT CAC CAG CCA GGT TC-3'
4	PV-sil-HpaI-R	5'-GAA CCT GGC TGG TGA TGT TaA CTA TCC AAC CCT TC-3'
5	pRLuc-SpeI-F	5'-GCG ACT AGT TAT TAT AAC TAG GAA CTA TGA AGA CAC CAC AAC AGT GCT AGC TAC CCT GGC CCT TC
6	pMo-BglII-F	5'-GAA GTG GAG ATC TTG GAT GCC AAA GCG-3'
7	3D-AflIII-R	5'-AAA GTC TGT CTT AAG CCT GGG ATC G-3'
8	PV-sil-SacII-F	5'-CGG TTC ACA CGG GTT TGC cGC GGC CCT GAA GCG A -3'
9	PV-sil-SacII-R	5'-TCG CTT CAG GGC CGC gGC AAA CCC GTG TGA ACC G-3'
10	PV-3C-D5A-F	5'-CAA GGA CCA GGG TTC gca TAC GCA GTG GCT ATG -3'
11	PV-3C-D5A-R	5'-CAT AGC CAC TGC GTA tgc GAA CCC TGG TCC TTG -3'
12	PV-3C-E24A-F	5'-GTT ACA GCA ACT ACT AGT AAG GGA gcc TTC ACT ATG TTA GGA GTC CAC G -3'
13	PV-3C-E24A-R	5'-GGT GGA CTC CTA ACA TAG TGA Agg cTC CCT TAC TAG TAG TTG CTG TAA C-3'
14	PV-3C-D32A-F	5'-CAC TAT GTT AGG AGT CCA Cgc gAA CGT GGC TAT TTT ACC AA-3'
15	PV-3C-D32A-R	5'-TTG GTA AAA TAG CCA CGT Tcg cGT GGA CTC CTA ACA TAG TG -3'
16	PV3C-E45A-F	5'-ACG CTT CAC CTG GTg cca GCA TTG TGA TCG ATG GC -3'
17	PV3C-E45A-R	5'-GCC ATC GAT CAC AAT GCT ggc ACC AGG TGA AGC GT -3'
18	PV-3C-D50A-F	5'-ACG CTT CAC CTG GTG AAA GCA TTG TGA Tcg cgG GCA AAG TGG AG -3'
19	PV-3C-D50A-R	5'-CTC CAC TTC TTT GCC cgc GAT CAC AAT GCT TTC A -3'
20	PV-3C-E53/E55A-F	5'-GTG ATC GAT GGC AAA gcc GTG gcc ATC TTG GAT GCC A -3'
21	PV-3C-E53/E55A-R	5'-TGG CAT CCA AGA Tgg cCA Cgg cTT TGC CAT CGA TCA C -3'
22	PV-3C-D58/E63A-F	5'-GAA GTG GAG ATC TTG gcg GCC AAA GCG CTC gcc GAT CAA GCA GGA ACC AAT C-3'
23	PV-3C-D58/E63A-R	5'-GAT TGG TTC CTG CTT GAT Cgg cGA GCG CTT TGG Ccg cCA AGA TCT CCA CTT C -3'
24	PV-3C-D64A-F	5'-GCC AAA GCG CTC GAA gca CAA GCA GGA ACC AAT CT -3'
25	PV-3C-D64A-R	5'-AGA TTG GTT CCT GCT Tgt gct TCG AGC GCT TTG GC -3'
26	PV-3C-E71A-F	5'-GCA GGA ACC AAT CTT gcc ATC ACT ATA ACT ACT C -3'
27	PV-3C-E71A-R	5'-GAG TGA TTA TAG TGA Tgg cAA GAT TGG TTC CTG C -3'
28	PV-3C-E81A-F	5'-CAC TAT AAT CAC TCT AAA GAG AAA Tgc tAA GTT CAG AGA CAT TAG ACC ACA -3'
29	PV-3C-E81A-R	5'-TGT GGT CTA ATG TCT CTG AAC Tta gca TTT CTC TTT AGA GTG ATT ATA GTG -3'
30	PV-3C-D85A-F	5'-GAG AAA TGA AAA GTT CAG Agc gAT TAG ACC ACA TAT AC -3'
31	PV-3C-D85A-R	5'-GTA TAT GTG GTC TAA Tcg cTC TGA ACT TTT CAT TTC TC -3'
32	PV-3C-E96/D99A-F	5'-ACC TAC TCA AAT CAC Tgc cAC AAA Tgc gGG AGT CTT GAT CGT G -3'
33	PV-3C-E96/D99A-R	5'-CAC GAT CAA GAC TCC cgc ATT TGT ggc AGT GAT TTG AGT AGG T -3'
34	PV-3C-E121A-F	5'-GTC GGT GCT GTG ACT gcc CAG GGA TAT CTA AAT CTC -3'
35	PV-3C-E121A-R	5'-GAG ATT TAG ATA TCC CTG ggc AGT CAC AGC ACC GAC -3'
36	GSSG-6H-EcoRI-R	5'-CCG GAA TTC CCA TGG CTA TTA ATG GTG GTG ATG GTG GTG ACC AGA GGA TCC -3'
37	pMo-R455A-F	5'-TAC TCA ACA TTG TAC gct CGT TGG CTT GAC TCA TTT TAG-3'
38	pMo-R455A-R	5'-CTA AAA TGA GTC AAG CCA ACG agc GTA CAA TGT TGA GTA-3'
39	pMo-EcoRI-F	5'-GAA TTA AAT CAT CGA TGA ATT CGG GCC C-3'
40	pUC18-PHBKSE-Top	5'-GGT TAA CGG ATC CGG TAC CAG ATC TCC GCG GG-3'
41	pUC18-PHBKSE-Bot	5'-AAT TCC CGC GGA GAT CTG GTA CCG GAT CCG TTA ACC TGC A-3'

A subclone, pUC18-3A-3C-HpaI-SacII, was created to facilitate mutagenesis. To create this plasmid, pUC18-3CD-BglII-EcoRI (45) was digested with PstI and EcoRI to remove the 3C-3D coding region. Oligonucleotides 40 and 41 (Table 1) were annealed to form a linker containing HpaI and SacII sites with PstI and EcoRI ends. This linker was ligated into the digested pUC18-3C-3D-BglII-EcoRI. The HpaI to SacII insert from pRLucRA, containing the 3B, 3C, and part of the 3A PV coding region, was cloned into the newly introduced restriction sites of this plasmid to form pUC18-3A-3C-HpaI-SacII.

The QuikChange® site-directed mutagenesis kit (Stratagene) was employed to introduce mutations into 3C-coding sequence with oligonucleotides 10–35 (Table 1). The resulting plasmids were used as templates for PCR with oligonucleotides 4 and 8 (Table 1). The PCR product was inserted into the SacI and HpaII sites of pMoRA-HpaI-SacII and pRLucRA-HpaI-SacII to produce pMoRA-HpaI-SacII-3C-acidic-to-alanine and pRLucRA-HpaI-SacII-3C-acidic-to-alanine, respectively.

Introduction of the R455A mutation into the 3D thumb subdomain in the viral cDNA required overlap extension PCR by using oligonucleotides 2 and 37–39 (Table 1) and the viral cDNA, pMoRA, as the template. The PCR product was digested with MfeI and EcoRI and subcloned into the intermediate plasmid, pUC18-BglII-EcoRI-3CD (referred to as pUC-3CD in Ref. 45). From this subclone, the fragment between ApaI and AvrII

was cloned into pRLuc-HpaI-SacII to yield the thumb mutant replicon (pRLuc-HpaI-SacII-3D-R455A). To introduce the mutation into pMoRA-HpaI-SacII, the fragment between the ApaI and SacII sites from the pRLuc-HpaI-SacII-R455A plasmid was digested, gel-purified, and cloned into pMoRA-HpaI-SacII to yield pMoRA-HpaI-SacII-R455A. To introduce the R455A mutation into the pRLucRA-HpaI-SacII-3C-acidic-to-alanine and pMoRA-HpaI-SacII-3C-acidic-to-alanine plasmids, the fragment between the ApaI and SacII sites from the pRLuc-HpaI-SacII-R455A plasmid was digested, gel-purified, and cloned.

Subgenomic Replicon Assays—RNA replicon transcripts were prepared as described previously (41). RNA transcripts (5 μ g) were electroporated into HeLa cells (1.2×10^6 in 400 μ l PBS) as described previously (41), and these electroporated cells were immediately transferred to 5.6 ml of pre-warmed (37 °C) media (DMEM/F-12). 500- μ l aliquots were prepared in microcentrifuge tubes and incubated on a rocker at 37 °C. At each time point (0, 2, 4, 6, 8, and 10 h), the cells were pelleted by centrifugation at $14,000 \times g$ for 2 min, and 100 μ l of cell culture lysis reagent (Promega) was added to the cell pellet. Lysates were left on ice at 4 °C until all time points were collected. Assays were performed by mixing 10 μ l of lysate with 10 μ l of luciferase assay substrate (Promega), and luciferase quantification was carried out as described by the supplier with a Junior

PV 3C Residues Required for VPg Uridylylation

LB 9509 luminometer (Berthold). Assays performed in the presence of 3 mM guanidine HCl, a reversible inhibitor of PV RNA replication (46–48), were used as negative controls.

In Vitro Translation Assays—RNA replicon transcripts were synthesized as described above. Translation reactions were carried out at 30 °C for 2 h in the presence of 1 μ Ci of [35 S]methionine (Amersham Biosciences) with HeLa S10 translation mixtures as described previously (41, 49, 50). The mixtures contained 60% by volume S10, 10% by volume initiation factor (rabbit reticulocyte lysate, Promega), 10% by volume 10 \times nucleotide mixture (10 mM ATP, 2.5 mM GTP, 2.5 mM UTP, 600 mM KCH₃CO₂, 300 mM creatine phosphate, 4 mg/ml creatine kinase, and 152 mM HEPES, pH 7.5), 2 mM guanidine HCl, and 4 μ g/ml replicon RNA. After 2 h of incubation at 30 °C, samples (5 μ l) were mixed with 30 μ l of SDS-PAGE sample buffer (2% SDS, 62.5 mM Tris-HCl, pH 6.8, 20% glycerol, 0.5% β -mercaptoethanol, and 0.1% bromophenol blue). The samples were heated at 90 °C for 5 min, and samples (5 μ l) were loaded on 12.5% SDS-polyacrylamide gels. Gels were fixed and dried, and the radiolabeled proteins were detected by phosphorimaging.

Virus Isolation, Virus Titer, and One-step Growth Curves—Viral RNA transcripts were synthesized as described previously (41). HeLa cells (1.2×10^6 , 400 μ l in PBS) were transfected with 5 μ g of viral RNA transcript as described above for the subgenomic replicon assays. Electroporated cells were immediately transferred to 400 μ l of pre-warmed (37 °C) media (DMEM/F-12) and added to HeLa cell monolayers (100 mm dishes) with 9.2 ml of DMEM/F-12 media. After incubation at 37 °C for 2 days, viruses were harvested by three repeated freeze-thaw cycles and used as stocks for analysis of plaque assays. The virus was serially diluted in PBS (10^{-2} , 10^{-4} , 10^{-5} , 10^{-6} , and 10^{-7}), and 100 μ l of each dilution was placed on cells (6×10^5 cells each) in 6-well dishes. 200 μ l of PBS was added to each well, and the mixture was incubated for 20 min at room temperature to allow the virus to adsorb to the cells. PBS was replaced with 3 ml of 1 \times DMEM/F-12 plus 10% fetal bovine serum, and 1% agarose was added to each well. After 2 days of incubation, the agarose overlay was removed, and the cells were stained with crystal violet. Plaques were counted to determine virus titer. To analyze one-step virus growth, cells in 6-well plates were infected with virus at a multiplicity of infection of 10. After a 20-min incubation at room temperature to allow virus to adsorb, cells were washed with PBS to remove excess virus. The cells were incubated at 37 °C for 0, 1–4, 6, and 8 h post-infection. Virus was harvested by three repeated freeze-thaw cycles, and virus titers were performed by plaque assays for the given time point.

Infectious Center Assays—Infectious center assays were performed as described previously (41). Briefly, HeLa cells were transfected with 5 μ g of viral RNA transcript, and these cells were serially diluted and plated onto HeLa cell monolayers. Four hundred μ l of DMEM/F-12 was added to each well. Cells were allowed to adsorb to the plate for 1 h at 37 °C, and then the medium/PBS was aspirated. Cells were covered with 3 ml of 1 \times DMEM/F-12 plus 10% fetal bovine serum and 1% agarose. After 2 days of incubation, the agarose overlay was removed, and the cells were stained with crystal violet.

Construction of PV 3C Expression Plasmids—The expression vectors containing WT or mutated PV 3C sequence were made using overlap-extension PCR with pET26Ub-3C-C147G-CHIS (41) as template. First, two PCR fragments were amplified using oligonucleotides 8, 36, and 10–35 (Table 1), and then the two fragments were used as templates for amplification of a new fragment using oligonucleotides 8 and 36 (Table 1). The fragment between SacII and EcoRI sites was cloned into pET26Ub-3C-C147G-CHIS plasmid to yield pET26Ub-3C-C147G-CHIS derivatives.

Expression and Purification PV 3C Derivatives—*Escherichia coli* BL21(DE3)pCG1 cells (51) were transformed with the pET26Ub-3C-C147G-CHIS derivative for protein expression. BL21(DE3)pCG1 cells containing the pET26Ub-3C-C147G-CHIS plasmid were grown in 100 ml of media (NZCYM) supplemented with kanamycin (25 μ g/ml), chloramphenicol (20 μ g/ml), and dextrose (0.4%) at 37 °C until an A_{600} of 0.8–1.0 was reached. Cells were then induced by adding isopropyl β -D-thiogalactopyranoside (0.5 mM final) and grown at 25 °C for 4 h. Cells were harvested by centrifugation (6000 \times g, 10 min), and the pellets were suspended in 4 ml of lysis buffer (100 mM potassium phosphate, pH 8.0, 20% glycerol, 10 mM β -mercaptoethanol, 500 mM NaCl, 2.8 μ g/ml pepstatin A, 2.0 μ g/ml leupeptin). The cell suspension was lysed by passing through a French press (SIM-Aminco). After lysis, phenylmethylsulfonyl fluoride and Nonidet P-40 were added to final concentrations of 2 mM and 0.1%, respectively. Lysates were clarified by centrifugation for 30 min at 75,000 \times g at 4 °C. The supernatants were then loaded onto nickel-nitrilotriacetic acid spin columns (Qiagen). The columns were washed twice with 600 μ l of buffer A (50 mM HEPES, pH 7.5, 0.1% Nonidet P-40, 20% glycerol, 10 mM β -mercaptoethanol) containing 500 mM NaCl and 50 mM imidazole. Proteins were eluted with 500 mM NaCl in buffer A containing 500 mM imidazole. The eluted pooled fractions were dialyzed against 1 liter of dialysis buffer (buffer A with 150 mM NaCl) at 4 °C for 3 h. After dialysis, protein concentration was determined at 280 nm in 6 M guanidine HCl, pH 6.5, using the extinction coefficient 0.007680 μ M $^{-1}$ cm $^{-1}$. Protein samples were analyzed on a 15% SDS-PAGE, which was stained with SYPRO Ruby stain (Invitrogen). The stained gel was scanned using a Typhoon variable mode imager (Amersham Biosciences). This approach permitted concentration of 3C to be determined by using a reference protein, thus excluding contributions of contaminants to the absorbance at 280 nm.

VPg Uridylylation Assays—VPg uridylylation assays were performed essentially as described previously (41). The reaction mixture contained 1 μ M 3C (WT or mutant), 1 μ M PV 61-nucleotide oril, and 10 μ M VPg in reaction buffer (50 mM HEPES, pH 7.5, 5 mM magnesium acetate, 10% glycerol, 10 mM β -mercaptoethanol, 0.04 μ M [α - 32 P]UTP (6,000 Ci/mmol) and 10 μ M unlabeled UTP). All reactions were adjusted to a final concentration of 20 mM NaCl. Reaction mixture was preheated at 30 °C for 5 min. Reactions were initiated by addition of PV 3Dpol to 1 μ M. All enzymes were diluted immediately prior to use in enzyme dilution buffer (50 mM HEPES, pH 7.5, 10 mM β -mercaptoethanol, and 20% glycerol). After incubation at 30 °C for 30 min, the reaction was stopped by the addition of an equal volume (5 μ l) of gel loading buffer (100 mM EDTA, 75%

formamide, 0.025% bromophenol blue and 0.025% xylene cyanol). The quenched samples (5 μ l) were analyzed by Tris-Tricine SDS-PAGE. Gels contained 15% acrylamide and 0.4% bisacrylamide. The cathode buffer (upper chamber) contained 0.1 M Tris, 0.1 M Tricine, and 0.1% (w/v) SDS; the anode buffer contained 0.2 M Tris-HCl, pH 8.9. Gels were run at 80 watts (for a 33–39-cm gel) for 2.5 h. The incorporation of [α - 32 P]UMP was visualized by using a PhosphorImager and quantified by using ImageQuant software.

Fluorescence Polarization Assays—Experiments were performed using a Beacon fluorescence polarization system (GE Healthcare) as described previously (13). Assays were performed by mixing various concentrations of PV 3C (WT or mutant) with 0.1 nM 3'-fluorescein-labeled PV oriI (29 nucleotides) in binding buffer (1 mM HEPES, pH 7.5, and 20 mM NaCl). Protein-RNA complexes were incubated for 30 s at 25 °C. Binding of PV 3C was measured by the change in polarization (ΔmP).

Construction of the Molecular Model for the 3C-3Dpol Complex—The atomic coordinates for PV 3C (Protein Data Bank 1L1N) and PV 3Dpol (Protein Data Bank 1RDR; partial structure missing the flexible fingers subdomain) were used as input files submitted to the GRAMM server to do the docking. The program GRAMM performs an exhaustive six-dimensional search through the relative translations and rotations of the molecules. The 3C molecule worked as the template and 3Dpol as the ligand in the docking run. Outputs for the top 10 solutions from the server were investigated carefully using graphics. The model that was most consistent with the available molecular genetic and biochemical data was chosen for further refinement. The 3C dimer was placed in a complex with the full structure of 3Dpol (Protein Data Bank 1RA6; which possesses the fingers subdomain missing from the 1RDR coordinates). The 1RA6 structure was superimposed on top of the docked 3Dpol by using the program O (52). Residues in 1RA6 that had been mutated to produce crystals were returned to the wild-type amino acids by using the program O. To alleviate the apparent clashes between the 3C and the parts of the 3Dpol structure not included in the original docking, the model was further subjected to energy minimization using the CHARMM force field in the NAMD package (53). The input files for the energy minimization were prepared using the VMD program (54). The minimization was stopped after 10,000 steps using the conjugate gradient minimizer; the relaxed structure was checked for unreasonable interactions by visual inspection and used as the final model.

RESULTS

Rationale—The first crystal structure of the RNA-dependent RNA polymerase (RdRp) from PV, 3Dpol, revealed extensive interactions between the back of the thumb subdomain of one 3Dpol molecule and the back of the palm subdomain of a second molecule that led to formation of fibers of 3Dpol in the crystal (55). Since this time, numerous studies have been designed to prove a function for 3Dpol fibers (56–58). Interestingly, PV mutants containing changes in 3Dpol-coding sequence designed to prevent fiber formation exhibit different biological phenotypes in cell culture (41). For example, changes

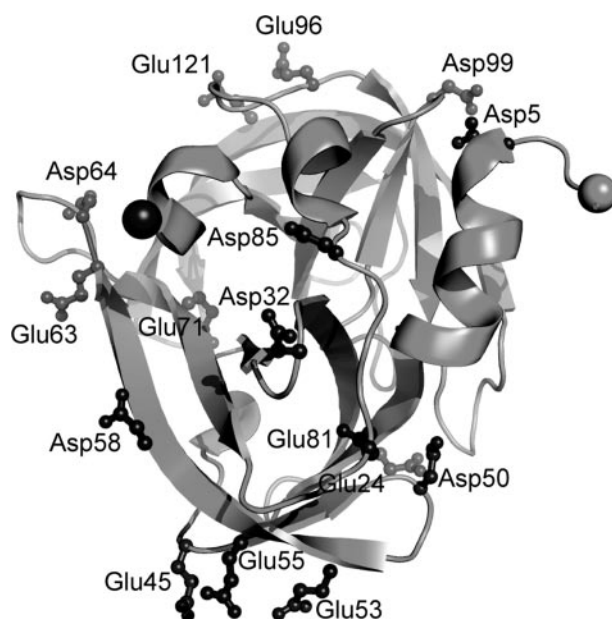


FIGURE 2. Solvent-accessible acidic amino acid residues of PV 3C. The structure of PV 3C (Protein Data Bank code 1L1N) is shown. The residues targeted for mutational analysis are labeled and shown as ball-and-sticks. The amino and carboxyl termini are displayed as light and dark spheres, respectively.

to the back of the thumb subdomain of 3Dpol are lethal to virus production because of a severe RNA synthesis defect (41, 42); however, comparable changes to the back of the palm subdomain produce viable virus (41). Specifically, a PV mutant encoding a 3Dpol enzyme in which both Arg-455 and Arg-456, two residues on the back of the thumb of 3Dpol, are mutated to Ala (3Dpol-R455A/R456A) is inviable (42). In the context of a subgenomic replicon, these amino acid substitutions prevent RNA synthesis (41). Studies of 3Dpol-R455A/R456A and related derivatives *in vitro* show the inability of these enzymes to form fibers *in vitro* without any change in the RdRp activity on RNA-primed templates (41). However, these derivatives are incapable of being stimulated by 3C(D) in oriI-templated VPg uridylylation experiments (41). This observation provided the first hint that a physical interaction between the back of the thumb of 3Dpol and 3C(D) exists that functions during VPg uridylylation (41). Subsequent studies provided additional functional and physical evidence for the existence of this interaction (13).

Because at least one Arg residue of 3Dpol participated in the interaction with 3C (41) and this interaction appeared to be quite sensitive to the concentration of salt employed (38), we hypothesized that at least one acidic amino acid residue of 3C participated in the interaction with 3Dpol. If this hypothesis is correct, then by changing this residue to Ala, a PV mutant would be created that should exhibit a phenotype comparable with 3Dpol-R455A/R456A PV mutant described above. Of course, any 3Dpol-interacting residue of 3C would be expected to reside on the surface of the protein. As shown in Fig. 2, 16 acidic amino acids exist on the surface of 3C. Proposed functions exist for many of these residues based on proximity to residues known to be involved in the RNA binding or protease activity of the protein (Table 2). In addition, some of these res-

PV 3C Residues Required for VPg Uridylylation

idues are located at the interface of the 3C dimer observed crystallographically, thus implying function (Table 2) (59). However, six of these residues do not have any known function (Table 2). Therefore, a surface acidic-to-alanine mutagenesis approach had the potential not only to identify the surface of 3C that interacts with 3Dpol but also to test experimentally the proposed functions of several other surfaces of 3C.

Study Design—All surface acidic amino acid residues of 3C were changed individually (single in Table 2) or in combination (double in Table 2) by site-directed mutagenesis of a shuttle vector containing 3C-coding sequence that permitted rapid subcloning of mutated DNA fragments into plasmids containing a PV genomic cDNA, a PV subgenomic replicon cDNA, or PV 3C-coding sequence under the control of a T7 RNA polymerase promoter. These constructs permit production of infectious virus in HeLa cells, evaluation of RNA synthesis in HeLa cells, or expression of 3C protein in *E. coli*, respectively.

PV 3C(D) has two well established functions during the PV life cycle. 3C(D) is a protease responsible for cleavage of the viral polyprotein (1, 2, 15). 3C(D) is an RNA-binding protein that recognizes, in addition to or1, replication elements at the 5'- and 3'-ends of the genome (17, 19–21, 23, 27, 31). However, functions for 3C(D) before and after RNA synthesis are also beginning to emerge (60–65). Because we were interested in identifying all phenotypes associated with these mutants, a

comprehensive analysis of the mutants was performed as described under "Experimental Procedures." The specific infectivity of PV genomic RNAs encoding the various 3C mutants was determined by infectious center assay. Kinetics of virus production under one-step growth conditions was determined for those alleles exhibiting a WT phenotype by infectious center assay. RNA synthesis was measured indirectly for all mutants by using the subgenomic replicon expressing luciferase. Proteolytic processing was evaluated by monitoring processing of the viral polyprotein produced by *in vitro* translation of subgenomic replicon RNA in a HeLa cell-free extract. Purified 3C proteins were evaluated for RNA binding and VPg uridylylation activities. Mutants of most interest to us here are those with growth defects because of defects in RNA synthesis unrelated to defects in proteolytic processing or RNA binding and exhibiting defects to VPg uridylylation *in vitro*.

Specific Infectivity by Infectious Center Assay—PV genomic RNAs encoding each of the 13 3C mutants were prepared by *in vitro* transcription of mutated PV genomic cDNAs. RNAs were transfected into HeLa cells by electroporation. Transfected cells were diluted, plated onto a monolayer of HeLa cells, covered with an agarose overlay, and incubated for 2–3 days at 37 °C. Monolayers were stained with crystal violet to visualize plaques. Specific infectivity (plaques formed per μ g of RNA) was calculated and reported as values relative to WT RNA (Table 3). Three phenotypes were observed. The specific infectivity of eight of the mutated RNAs (D5A, D32A, E45A, D50A, E53A/E55A, D58A/E63A, E81A, and E121A) was equivalent to WT RNA. The specific infectivity of two of the mutated RNAs (E24A, E96A/D99A) was reduced by 100-fold relative to WT RNA. Infectious virus could not be recovered from three of the mutated RNAs (D64A, E71A, D85A).

Kinetics of Virus Growth—The kinetics of virus growth were evaluated for PV mutants whose specific infectivity was equivalent to WT PV. All of these mutants exhibited a reduced rate of virus growth; a representative set of data is presented in Fig. 3. The titer of each mutant at 6 h post-infection was compared

TABLE 2
Poliovirus 3C residues targeted for mutational analysis

PV 3C mutant	Targeted residue	Proposed function	Type of substitution
1	Asp-5	RNA recognition	Single
2	Glu-24	None	Single
3	Asp-32	RNA recognition	Single
4	Glu-45	Intermolecular contacts	Single
5	Asp-50	None	Single
6	Glu-53/Glu-55	None/intermolecular contacts	Double
7	Asp-58/Glu-63	Intermolecular contacts	Double
8	Asp-64	None	Single
9	Glu-71	Proteolytic active site	Single
10	Glu-81	RNA recognition	Single
11	Asp-85	RNA recognition	Single
12	Glu-96/Asp-99	None	Double
13	Glu-121	None	Single

TABLE 3
Summary of phenotypes observed for surface acidic-to-alanine mutants of 3C

All values are presented as a fraction of WT where indicated.

Mutation	Specific infectivity ^a	Virus growth ^b (6 h)	RNA synthesis ^c (4 h)	Processing	3C protein solubility	VPg-pU(pU) uridylylation ^d	Or1 binding ^e
D5A	1	0.02	0.3	+	+	0.4	0.5
E24A	0.01	ND ^f	0.1	+	+	2.0	1.1
D32A	1	0.2	0.6	+	+	1.2	1.1
E45A	1	0.6	0.9	+	+	0.1	0.9
D50A	1	0.8	0.5	+	+	1.4	0.9
E53A/E55A	1	0.1	0.4	+	+	1.0	1.0
D58A/E63A	1	0.1	0.6	+	+	0.8	0.7
D64A	0	ND	0	+	+	0.9	0.7
E71A	0	ND	0	–	+	0.1	0.8
E81A	1	0.1	0.6	+	+	0.9	1.0
D85A	0	ND	0	–	–	ND	ND
E96A/D99A	0.01	ND	0.1	+	+	0.3	0.8
E121A	1	0.6	0.6	+	+	0.7	0.8

^a WT showed a specific infectivity of 6×10^4 plaque-forming units/ μ g RNA.

^b WT showed a titer of 1.5×10^7 plaque-forming units/ml at 6 h post-infection.

^c WT showed 4×10^5 RLU/ μ g at 4 h post-transfection.

^d WT showed 2 μ M VPg-pU(pU) uridylylation in 30 min.

^e WT showed a ΔmP value of 110 at 150 nm.

^f ND means not determined.

with that for WT PV, revealing a 2–50-fold reduction in the rate of virus growth for these mutants (Table 3).

Kinetics of RNA Synthesis—Because 3C protein and 3C-containing precursor proteins play roles in the virus life cycle before, during, and after RNA synthesis, it was important to identify those 3C mutants whose growth phenotypes were attributable to RNA synthesis. For these experiments, a subgenomic replicon encoding luciferase instead of the viral capsid proteins was employed. This replicon permits the kinetics of RNA synthesis to be monitored indirectly by measuring the specific activity of luciferase as a function of time. Luciferase specific activity is expressed as relative light units observed per μg of total protein. Transfected replicon RNA can be translated to produce luciferase in the absence of replication. The signal that derives from translation of the transfected replicon RNA can be obtained by transfection of the replicon RNA into cells in

the presence of 3 mM guanidine hydrochloride, an inhibitor of PV RNA synthesis (46–48).

All of the 3C mutants were evaluated in the context of the subgenomic replicon. Replicon RNAs were transfected into HeLa cells. At 4 and 8 h post-transfection, cell extracts were prepared, and luciferase activity was measured. These two time points were chosen because they represent times in which replication is 50 or 100% complete for the WT replicon (Fig. 4). All of the mutated replicon RNAs exhibited a delay in the kinetics of RNA synthesis relative to WT replicon RNA (Fig. 4 and Table 3). As observed for the specific infectivity experiment, the mutants could be divided into three categories. Those mutants that failed to produce virus also failed to replicate; these are: D64A, E71A, and D85A. The D64A allele produced as much luciferase as WT replicon in the presence of guanidine HCl, suggesting that the stability and translatability of this RNA was normal. In contrast, the E71A and D85A alleles produced lower levels of luciferase at both time points evaluated, suggesting that stability and/or translatability of these RNAs may have been affected. One class of mutants exhibited a lower-than-expected reduction in replication efficiency relative to the observed kinetics of virus growth or specific infectivity. These are as follows: D5A, E24A, E53A/E55A, D58A/E63A, and E81A, E96A/D99A. These mutants may be defective in a post-replicative function of 3C or some precursor thereof in addition to having a function in replication. The final class of mutants exhibited reductions in RNA replication efficiency on par with that observed for the kinetics of virus growth. These are as follows: D32A, E45A, D50A, and E121A. These residues are likely only important for replication functions of 3C and/or its precursors.

Proteolytic Activity of 3C Mutants—To determine whether any of the growth and/or replication phenotypes were caused by inactivating 3C-dependent proteolysis, we performed *in vitro* translation experiments with subgenomic RNAs. Translation-competent HeLa extracts containing [^{35}S]Met were pro-

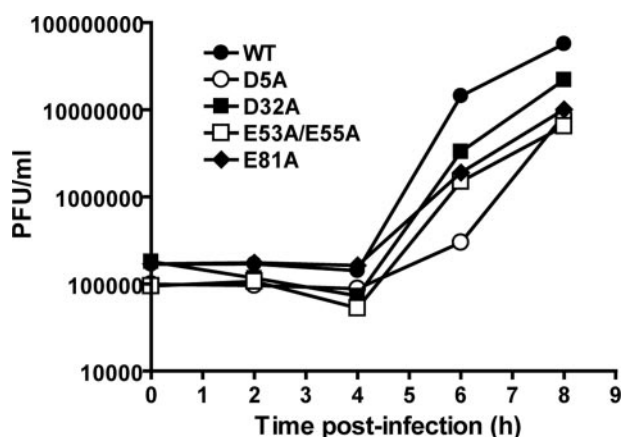


FIGURE 3. Kinetics of virus growth for selected PV 3C mutants. HeLa cells were infected at a multiplicity of infection of 10 with PV encoding WT or the indicated mutant 3C protein. The cells were incubated at 37 °C for 0, 1–4, 6, and 8 h post-infection. Virus was harvested by three repeated freeze-thaw cycles, and virus titers were performed by plaque assays on HeLa cells. Viral titer (plaque-forming units/ml) was plotted as a function of time post-infection.

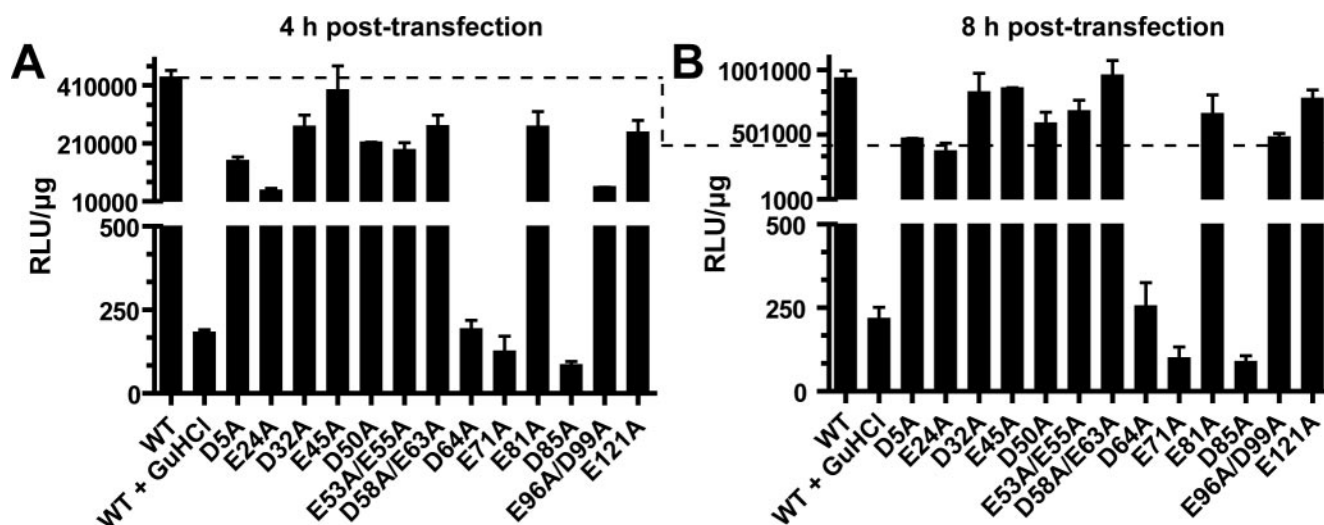


FIGURE 4. Kinetics of RNA synthesis using a luciferase-expressing, subgenomic replicon. HeLa cells were transfected with the indicated replicon RNA (5 μg) and incubated for 4 (A) or 8 h (B) post-transfection. Extracts were prepared and analyzed for luciferase activity. Luciferase specific activity is reported in relative light units (RLU) per μg of total protein in the extract. WT + guanidine HCl represents a control for translation of input RNA without replication. The dashed line indicates luciferase activity observed for WT at 4 h. The results are the average of two independent transfections of replicon RNA transcribed from two independent clones. Error bars indicate the standard deviation.

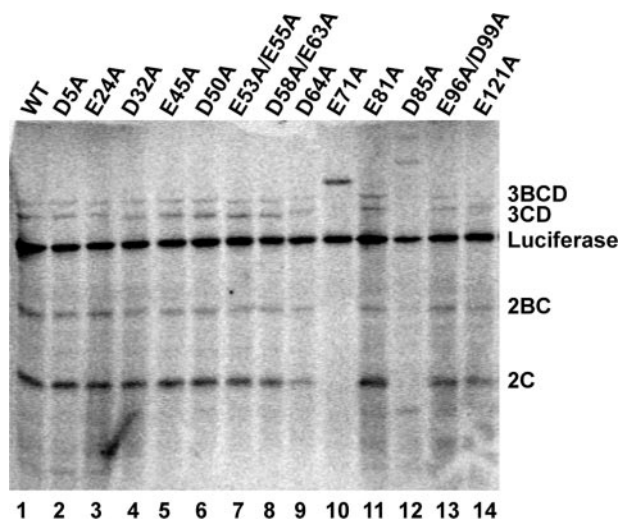


FIGURE 5. **Proteolytic processing activity of PV 3C mutants.** HeLa extracts containing [35 S]methionine were programmed with subgenomic replicon RNAs encoding the indicated 3C protein. After 2 h, samples were mixed with SDS-PAGE sample buffer and resolved by SDS-PAGE on a 12.5% acrylamide gel. Gels were fixed and dried, and the radiolabeled proteins were detected by phosphorimaging.

grammed with each of the mutated replicon RNAs. Labeled products were resolved by SDS-PAGE and visualized by phosphorimaging (Fig. 5). Luciferase is produced co-translationally by the virus-encoded 2A protease and serves as control for RNA stability and gel loading. The other P2 and P3 proteins are processed by 3C-dependent activities. With the exception of the E71A and D85A mutants, all other mutants exhibited WT levels of processing. Identical effects have been observed for other substitutions at these positions of 3C (66). Unfortunately, this experiment is not sensitive enough to reveal subtle differences in kinetics of proteolysis.

VPg Uridylylation—To identify 3C mutants with replication defects that could be attributable to VPg uridylylation, we expressed each of the 3C mutants in *E. coli*. With the exception of D85A protein, all other proteins were soluble. All 3C proteins contained a carboxyl-terminal hexahistidine tag. Soluble proteins were purified to greater than 80% purity in a single step by using a nickel-nitrilotriacetic acid-agarose spin column. A representative set of purified proteins is shown in Fig. 6A.

PV VPg uridylylation, *i.e.* production of VPg-pUpU and VPg-pU, can be recapitulated *in vitro* from purified component as follows: 3Dpol, 3C, oriI, VPg, and [α - 32 P]UTP. The ability of each protein to function in this reaction was measured. A representative experiment is shown in Fig. 6B. The uridylylation efficiency for all soluble 3C derivatives was determined in at least three different experiments. The average uridylylation efficiency for each derivative is shown in Table 3. Four of the 3C derivatives exhibited at least a 2-fold reduction in VPg uridylylation. These are as follow: D5A, E45A, E71A, and E96A/D99A. Two of the 3C derivatives, E24A and D50A, exhibited an increase in VPg uridylylation on the order of 2-fold greater than WT 3C. The remaining 3C derivatives did not exhibit a substantial difference (2-fold or greater) in VPg uridylylation activity relative to WT 3C.

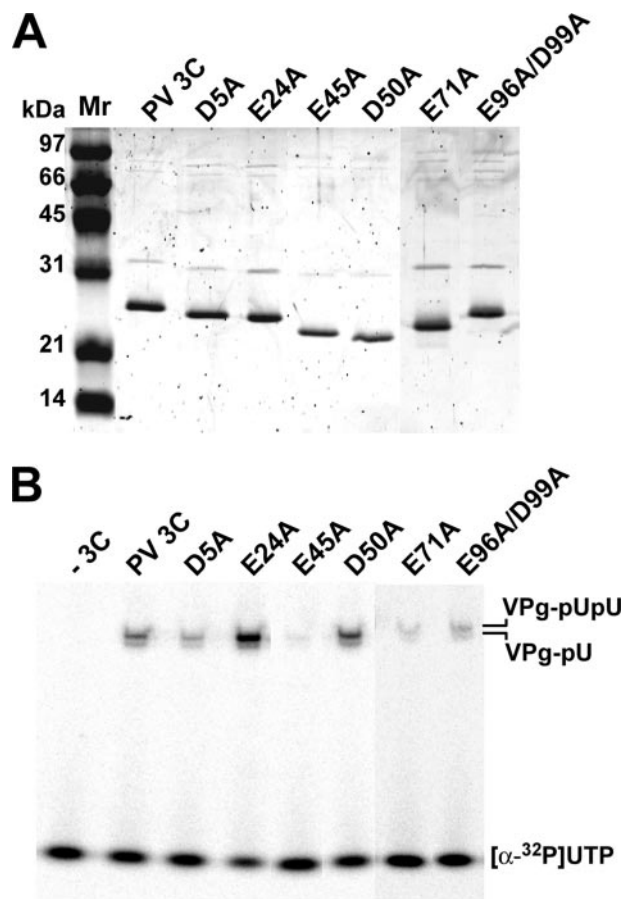


FIGURE 6. **VPg uridylylation activity of selected PV 3C mutants.** A, sypro-stained gel of spin column-purified proteins (0.1 μ g) employed in the VPg uridylylation experiment. The sypro-stained proteins were detected by using a Typhoon-8600 Variable Mode Imager. B, VPg uridylylation reactions were performed by using the indicated purified 3C derivative. Uridylylation products were resolved from [α - 32 P]UTP by using a 15% polyacrylamide gel and a Tris-Tricine buffer system. The $-3C$ lane indicates a reaction performed in the absence of 3C.

OriI Binding—The last experiment that we performed to screen the mutants was an RNA-binding experiment. 3C protein has two roles in VPg uridylylation, binding to oriI and recruitment of 3Dpol (13, 14). Changes in VPg uridylylation could be caused by changes in either activity. We used a fluorescence polarization assay to characterize binding of 3C derivatives to oriI (13). As shown in Fig. 7A, WT 3C was titrated into binding reactions containing fluorescein-labeled oriI under the same buffer conditions employed for VPg uridylylation. The change in fluorescence anisotropy (ΔmP) was plotted as a function of 3C concentration. The data were fit to a hyperbolic binding equation by using a nonlinear regression algorithm, yielding an equilibrium dissociation constant (K_d) value of 260 ± 40 nM. Each of the 3C derivatives was evaluated at a single protein concentration, 150 nM, which is in the linear range of the hyperbola. The observed fluorescence anisotropy was measured and compared with WT 3C (Fig. 7B and Table 3). Of the six 3C derivatives that exhibited changes in VPg uridylylation, only one of these (D5A) exhibited a reduction in oriI binding activity. Cross-linking experiments failed to report a change in 3C dimerization, which could also cause changes in oriI binding or 3Dpol recruitment (data not shown).

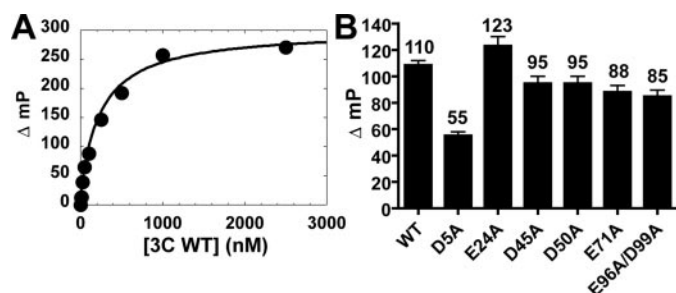


FIGURE 7. Oril binding by selected PV 3C derivatives. A, oril binding by WT 3C. 3'-Fluorescein-labeled oril RNA (29 nucleotides) was titrated with 3C. Binding was measured by monitoring the change in fluorescence polarization (ΔmP). The data were fit to a hyperbola. The K_d value is 260 ± 40 nM. B, oril binding by 3C derivatives. 3C protein (150 nM) was mixed with 3'-fluorescein-labeled oril RNA and the change in polarization (ΔmP) was measured. The results are the average of three independent binding experiments with error bars indicating the S.D.

The Surface of 3C Dimer Required for VPg Uridylylation Interacts with 3Dpol—Thus far this study has defined five residues that fit the criteria for 3Dpol-interacting residues: Glu-24, Glu-45, Glu-71, Asp-96, and Asp-99. Most appear on a single convex surface of the 3C dimer. We reasoned that if this is the surface that interacts with 3Dpol, then 3C mutants with changes on this surface might exhibit synthetic lethality in the context of 3Dpol-R455A, a mutant with a slow replication phenotype because of a defect in VPg uridylylation (38). The conceptual framework for this experiment is shown in Fig. 8A. Essentially, combining residues that contribute to the same function, stabilizing the same interface in this case, would be more deleterious than combining residues with different functions. For this experiment, three different 3C mutants were selected: E45A, E96A/D99A, and E53A/E55A. All three of these mutants exhibit equivalent reductions in virus growth and replication; however, only the first two are thought to contribute to an interaction with 3Dpol that is required for VPg uridylylation (Table 3). All three mutants replicate equivalently in a background that contains WT 3Dpol (Fig. 8B). In contrast, E45A and E96A/D99A are lethal to replication in the 3Dpol-R455A background (Fig. 8B). Importantly, E53A/E55A did not cause any additional defect to replication of the 3Dpol-R455A mutant (Fig. 8B). We conclude that these and related residues of 3C-containing precursors contribute to a surface employed for recruitment and retention of 3Dpol to the VPg uridylylation complex.

Structural Model for the 3C₂-3Dpol Complex—High resolution crystal structures for the PV 3C dimer and PV 3Dpol are available (59, 67). Having implicated a surface of the 3C dimer that interacts with 3Dpol, coupled with our previous studies that identified residues of 3Dpol essential for the interaction with the 3C dimer (13, 14), we were confident that we had sufficient information to begin to distinguish between mutually exclusive solutions of complexes identified by using computational approaches. We have employed a well established molecular docking algorithm (68) to obtain a structural model for the 3C₂-3Dpol complex. Ten solutions were returned. One solution was completely consistent with all of our molecular genetic and biochemical data (13, 14, 41).

The model is shown in Fig. 9. Both the thumb and fingers subdomains of 3Dpol interact with the "top" of the 3C dimer,

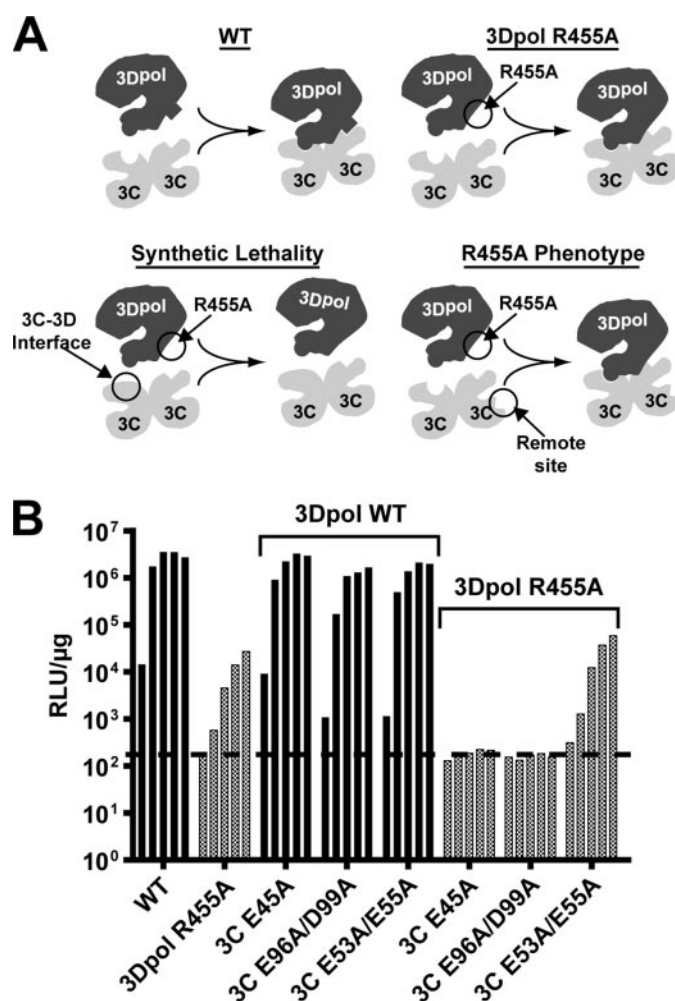


FIGURE 8. PV mutants encoding substitutions in 3C residues proposed to interact with 3Dpol exhibit synthetic lethality in a PV background producing 3Dpol R455A. A, conceptual framework for this experiment. (i) WT 3C₂ and 3Dpol interact via specific surface residues. (ii) R455A mutation in 3Dpol weakens 3C₂-3Dpol interaction and reduced replication occurs. (iii) R455A 3Dpol mutation combined with 3C₂ interaction surface mutation disrupts 3C₂-3Dpol interaction and prevents replication (synthetic lethality). (iv) R455A 3Dpol mutation combined with 3C₂ remote site (noninteraction surface) mutation results in 3C₂-3Dpol interaction and replication as in ii. B, replication of WT, 3Dpol-R455A, or 3C mutations as indicated in either 3Dpol-WT or 3Dpol R455A background. Luciferase activity (relative light units (RLU)/μg) was determined 2, 4, 6, 8, and 10 h post-transfection into HeLa cells. Dashed line indicates luciferase activity attributable to translation only. The 3C E45A and E96A/D99A mutants exhibit synthetic lethality in the 3Dpol R455A background, further confirming an interaction of these residues with 3Dpol.

the side containing the protease-active sites. The complex buries 1987 Å² of the solvent-accessible surface area. The complex has a nonplanar, interwoven interface with a high degree of complementarity between the surfaces of the 3C dimer and 3Dpol. Both side chain and backbone atoms contribute interactions to the interface. A channel is formed at the interface of the proteins (Fig. 9B). The channel is ~10 Å in diameter and 36 Å in length. These dimensions are consistent with accommodation of a single-stranded RNA molecule that is 10 nucleotides long.

The thumb of 3Dpol contributes most of the interactions to the interface, at least 12 amino acid residues (Fig. 9D). Worth noting is the presence of residues 406 and 455; these are known to be essential for VPg uridylylation (14, 32, 38, 41). In addition,

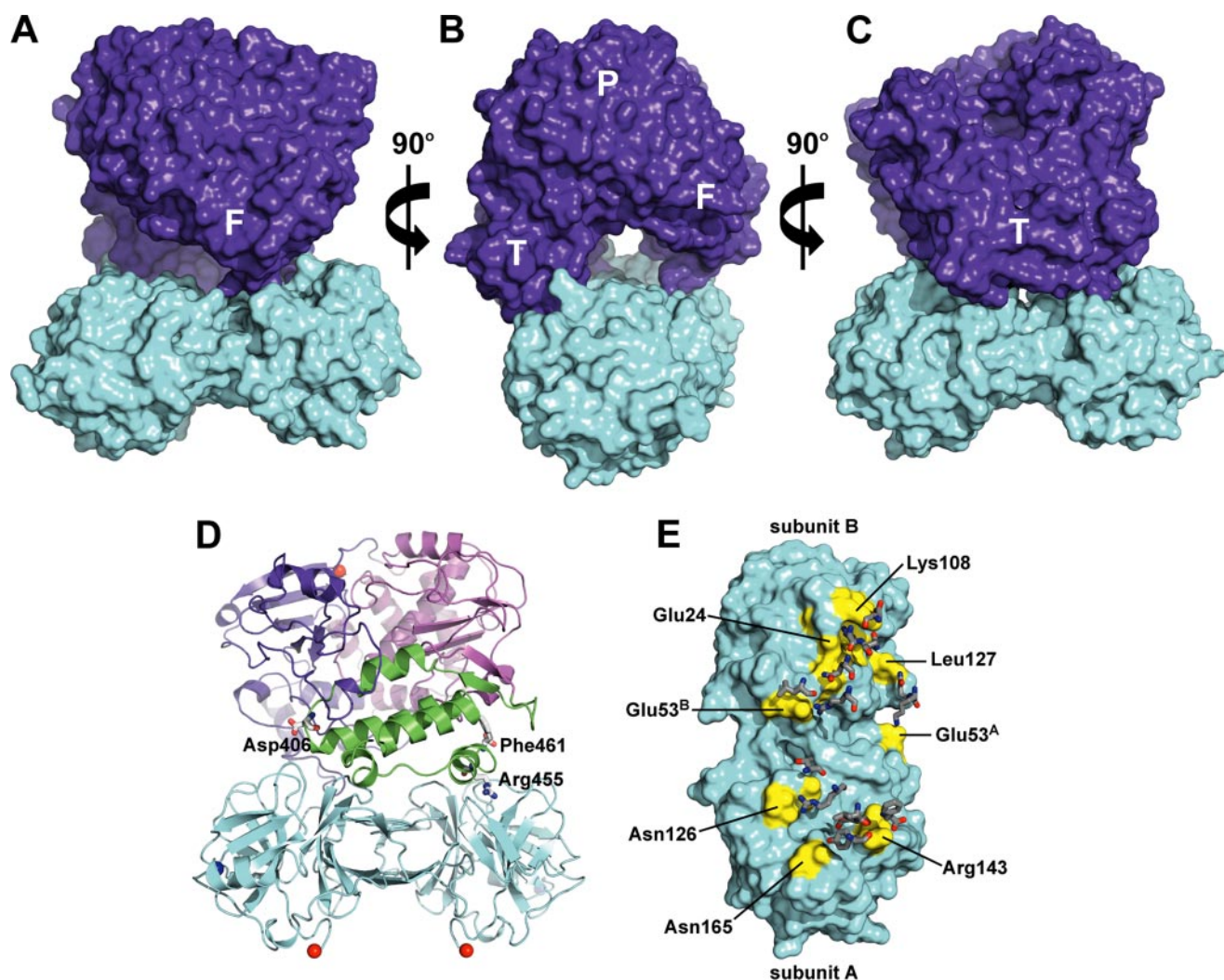


FIGURE 9. **Model of 3C₂-3Dpol complex.** *A*, surfaces of the 3C dimer and 3Dpol are shown in cyan and purple, respectively. The 3Dpol subdomains are abbreviated as follows: *F*, fingers; *T*, thumb; *P*, palm. *B*, same as in *A* with 90° rotation around the y axis. *C*, same as in *A* with 180° rotation around the y axis. *D*, model of 3C₂-3Dpol is shown rotated 180° around the y axis relative to the view in *A*; 3Dpol residues known to be required for VPg uridylylation are shown. These are Asp-406 (14, 32), Arg-455 (38, 41), and Phe-461 (69). *E*, residues of the 3C dimer that contribute to interaction with 3Dpol are shown in yellow. Selected 3C residues are shown for orientation. The complementary residues from 3Dpol are displayed as sticks. These interactions are listed in Table 4.

residue 461, the carboxyl-terminal residue, is located at the interface. A PV 3Dpol derivative that contains a GSSG-H₆ extension at the carboxyl terminus is as active as unmodified 3Dpol in RNA-primed synthesis (51) but completely lacks any VPg uridylylation activity.⁸ Only two residues of the fingers subdomain, Lys-133 and Gln-134, contribute directly to the interface.

The residues of 3C dimer at the interface are clustered in three patches (Fig. 9E). One patch is on subunit A of 3C and interacts with residues of the fingers subdomain of 3Dpol. The other two patches reside on both subunits A and B of 3C and interact with the thumb subdomain of 3Dpol. A complete list of the interactions is provided in Table 4.

DISCUSSION

The 5'-end of both plus and minus strand RNAs of all picornaviruses is linked to a protein, VPg, which is also referred to as 3B (1, 2). Linkage of VPg to picornaviral RNAs requires uridy-

TABLE 4
Side chain interactions in the 3C₂-3Dpol complex

3C ^A -3Dpol ^a	3C ^B -3Dpol	3C-3C ^b
Glu-53 to Lys-133	Leu-127 to Gln-134	Lys-22 to Glu-45
Asn-165 to Tyr-384	Lys-108 to Asp-406	Ser-42 to Glu-45
Gly-128 to Thr-452	Glu-24/Phe-25/Thr-106 to Arg-408	Asp-58 to Lys-60
Asn-126 to Arg-455	Lys-108/Tyr-109/Gly-145	Ile-56 to Ala-61
Arg-143 to Leu-458	Lys-108 to Asn-409	Glu-63 to Lys-78
Phe-461	Thr-19 to Gln-411	
Ala-144 to Asp-459	Glu-53 to Arg-415	Glu-55 ^A to Asn-69 ^B
	Glu-53 to Leu-446	Arg-130 ^A to Glu-55 ^B

^a The two subunits of the 3C-dimer are designated A and B.

^b Most of the interactions between the two monomers in the 3C dimer are symmetrical. Asymmetrical interactions are designated with the chain labels A/B.

lylation of VPg to form VPg-pUpU. This product then serves as primer for production of full-length plus and minus strand RNAs. All picornaviruses have a cis-acting replication element that we refer to as oril that serves as an efficient template for VPg uridylylation (3). The oril-templated VPg uridylylation reaction has been reconstituted *in vitro* from purified components for a variety of picornaviruses (5, 10–14). As a result,

⁸ H. B. Pathak, and C. E. Cameron, unpublished observations.

there is clear consensus on the virus-encoded protein factors that are required for this reaction. In a minimal system, in addition to the viral RNA-dependent RNA polymerase, 3Dpol, the RNA binding activity of 3C or some precursor thereof, for example 3CD, is required for efficient VPg uridylylation. The precise function for 3C(D) in VPg uridylylation is not known. As indicated in Fig. 1, we have recently proposed that a 3C(D) dimer binds to oriI, extending the loop for binding to the RNA-binding site of 3Dpol (13). Recruitment of 3Dpol to this complex and stability therein would be mediated by an interaction between the back of the thumb subdomain of 3Dpol and an undefined subdomain of 3C (13, 14). The goal of this study was to identify the 3Dpol-recruitment/retention subdomain of 3C. Again, this subdomain of 3C would likely function in the context of a precursor, for example 3CD.

Because arginine residues on the back of the thumb of 3Dpol were known to be required for recruitment to and/or retention in the VPg uridylylation complex (13, 14, 41), acidic residues on 3C seemed reasonable candidates for interaction with 3Dpol. Importantly, 16 solvent-accessible, acidic residues of 3C existed (Fig. 2). Many of these residues have either only implied function, for example intermolecular interactions based on structural information, or no known function (Table 2). We constructed a panel of PV mutants that encoded changes in 3C in which surface acidic residues were converted to alanine (Table 2). The biological and biochemical activities of the 3C derivatives were evaluated (Figs. 3–7). These data are summarized in Table 3. None of the mutants exhibited a wild-type phenotype in all assays (Table 3). Four classes of mutants were identified and are discussed below. Importantly, one of these classes exhibited all of the properties consistent with a surface of 3C involved in recruitment of 3Dpol to the VPg uridylylation complex.

Folding, Proteolysis, and RNA-binding Functions—The first class of mutants encoded changes at positions of 3C with established functions or at positions whose functions were not mechanistically insightful. Glu-85 appears to be important for folding of 3C, and formation of the protease-active site as this derivative produced an insoluble protein in *E. coli* (Table 3) and was unable to process the viral polyprotein in HeLa cells (Fig. 5). Glu-71 is a well known component of the catalytic triad of the protease-active site of 3C (59, 70), so it was not surprising that virus could not be recovered from the E71A mutant because of the proteolysis defect. However, as discussed below, unexpected roles for Glu-71 in VPg uridylylation exist.

Asp-32 has been shown to be required for *in vitro* assembly of the ribonucleoprotein complex that contains the cis-acting replication element at the 5'-end of the poliovirus (PV) genome (oriL) (17). That study did not report any biological analysis of this particular 3C derivative (17). Our data suggest that the oriI binding activity of 3C-D32A was equal to that observed for WT 3C (Table 3), and less than a 2-fold decrease was observed on replication of a subgenomic replicon RNA encoding this 3C derivative (Fig. 4). This apparent paradox can be interpreted in several ways. It is possible that precursor rather than processed forms of the proteins are employed for binding to these RNA elements *in vivo*, contributing independently to the RNA binding activity of 3C-containing precursors and suppressing RNA

binding defects in 3C observed *in vitro*. It is also possible that Asp-32 is involved in a protein-protein interaction with other proteins in the ribonucleoprotein complex. Loss of this interaction may preclude observation of the complex by using a gel mobility shift assay but only have a minor effect in cells for the reasons discussed above. Regardless of the explanation for the observed difference, this result clearly illustrates why a complete range of assays is required to achieve a clear understanding of picornaviral protein functions.

The amino terminus of 3C has been implicated in RNA binding (20).⁷ 3C-D5A exhibited a 2-fold reduction in oriI binding that was sufficient to explain the 2-fold reduction in VPg uridylylation as well as the 3-fold reduction in genome replication (Table 3). However, none of these phenotypes were sufficient to explain the 50-fold reduction in virus production, suggesting another function. In contrast, residues in the vicinity of Glu-121 have not been implicated in RNA binding. However, 3C-E121A exhibited a 20–30% reduction in oriI binding, causing a comparable reduction in VPg uridylylation and genome replication. These are the first PV mutants that exhibited a quantitative correspondence between VPg uridylylation activity *in vitro* and genome replication in cells. We have recently argued that PV produces far more VPg-pUpU than required for genome replication, thus preventing VPg uridylylation from affecting the kinetics of genome replication (14). This assertion may still be correct; the genome-replication phenotype associated with the D5A and E121A mutants may be a reflection of defects associated not only with oriI binding but also oriL and oriR binding.

Post-replication Functions—The second class of mutants exhibited defects in virus production that were more severe (greater than 5-fold) than defects associated with RNA synthesis (Table 3), suggesting that 3C(D) or precursors thereof function not only during replication but also after replication. These mutants were as follows: D5A, E53A/E55A, D58A/E63A, and E81A. The D64A mutant was dead and could not be studied, but it is likely that this mutant belongs to this group given its close proximity to several members of this class. By using a cell-free system for PV synthesis, Paul and co-workers (64, 65) have shown that addition of 3C(D) to these extracts stimulates a post-replication step in PV synthesis by greater than 100-fold. Currently, it is thought that 3CD stimulates maturation of the PV virion (64, 65). Similarly, it is possible that these amino acid substitutions alter the kinetics and/or specificity of capsid precursor processing, leading to problems with virion assembly and/or maturation. Although the mechanistic basis for this defect is not at all clear, these mutants should permit both genetic and biochemical approaches to be applied to this problem.

It is important to highlight the fact that this class of mutants failed to exhibit a phenotype by using an infectious center assay. There is no doubt that the infectious center assay is qualitative and really only measures viral RNA-induced cell death, not virus assembly or spread. However, such striking differences between the outcome of the infectious center assay and virus infectivity have never been reported, most likely because both assays are not generally employed in the same study. The reason for this difference is not clear. Our data show that a 10-fold reduction in the kinetics of virus assembly and/or spread is not

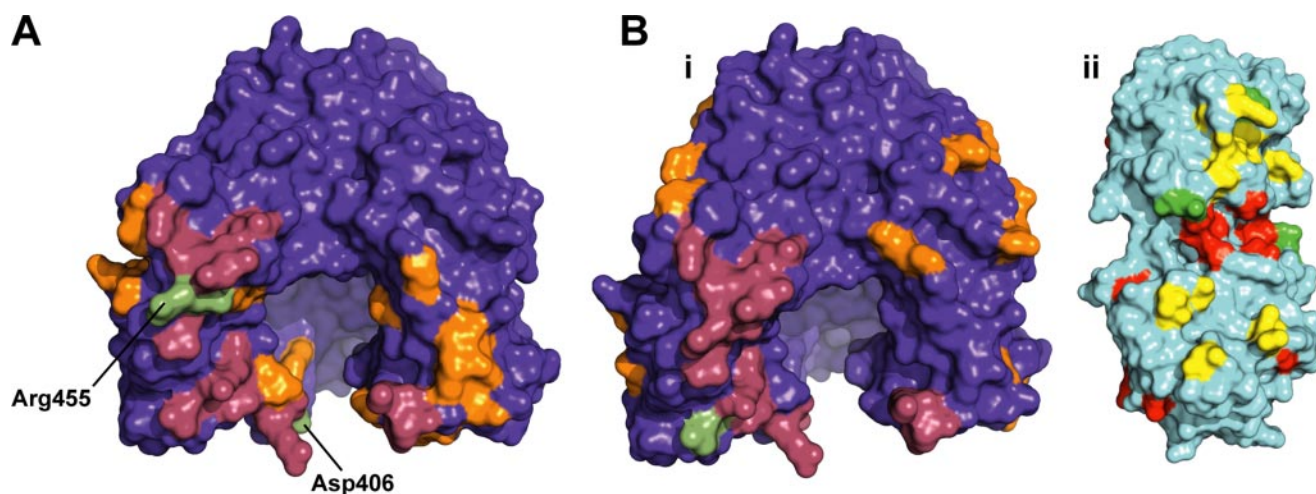


FIGURE 10. A, previously isolated 3Dpol mutants map to the 3C₂-interaction surface defined in this study. The 3Dpol surface is colored *purple*, and regions of 3Dpol involved in 3C₂-3Dpol interactions are shown in *raspberry*. 3Dpol mutants constructed as in Ref. 42 are shown in *orange*. Those that killed the virus include the following: Arg-128, Lys-383, Lys-405, Asp-406, Asp-412, Arg-455, and Arg-456. Those that caused a temperature-sensitive phenotype include the following: Glu-98, Asp-99, Asp-105, Glu-108, Arg-136, Asp-137, Glu-426, Glu-427, and Glu-428. Residues that overlap directly with those for which biochemical data exist are shown in *italic* above and shown in *green* on the structure. B, diversifying residues on 3C and 3Dpol map to the 3C₂-3Dpol interface. *i*, the 3Dpol surface is colored *purple*, and regions that interact with the 3C dimer are shown in *raspberry*. Diversifying residues of 3Dpol identified in Ref. 35 are shown in *orange*, including Met-86, Glu-93, Thr-138, Lys-200, Glu-254, Gly-259, Asp-260, Glu-369, Pro-385, Lys-431, and Ala-434. Residues identified in both studies are shown in *red*. *ii*, the 3C surface is colored in *cyan*, and regions that interact with 3Dpol are shown in *yellow*. Diversifying residues of 3C identified in Ref. 35 are shown in *red*, including Ser-21, Gly-44, Glu-45, Ser-46, Thr-68, Tyr-109, and Thr-120. Residues identified in both studies are shown in *green*.

detected by this assay. We speculate that as long as translation and genome replication of the genome is fast relative to the 2-day assay, even a cell infected with a reduced quantity of virus will die quite rapidly given the cytotoxicity of the viral proteins, especially the 3C and 3CD proteins.

Pre-replication Functions—The third class of mutants exhibited specific infectivity defects that were more severe (10-fold) than RNA synthesis. These mutants were E24A and E96A/E99A (Table 3). Given the discussion of the infectious center assay above, these mutants should be defective in translation or replication (directly or indirectly). Translation and processing appeared normal, at least in a cell-free extract (Fig. 5). The RNA binding activity of both 3C derivatives was on par with WT protein (Table 3). Because the proteolytic and RNA binding activities are the only known activities of 3C(D) or its precursors that could have an effect on translation and/or genome replication, these data may suggest more new functions for 3CD. It is well known that poliovirus genome replication can be inhibited by brefeldin A, an inhibitor of ER-to-Golgi trafficking (69, 71, 72). Recently, Ehrenfeld and co-workers (60–63) showed that introduction of 3CD protein into HeLa cell-free extracts caused stable association of a brefeldin A-targeted guanine-nucleotide exchange factors with membranes. Importantly, this activity of 3CD appears to be essential for genome replication, presumably by facilitating formation of the vesicular clusters that are induced by the virus and employed for genome replication (60–63). It is possible that the E24A and E96A/E99A mutants are defective in this novel pre-replication function of 3CD.

VPg Uridylylation Functions—The final class of mutants encoded 3C proteins that exhibited changes in VPg uridylylation activity that were unrelated to RNA binding activity (Figs. 6 and 7). These mutants were E24A, E45A, D50A, E71A, and E96A/E99A. It was the isolation of this class of mutants that was

the primary motivation for this study, identification of a 3C surface that interacts with 3Dpol. Interestingly, 3C-E24A and 3C-D50A exhibited gain-of-function for VPg uridylylation (Fig. 7). As discussed above, E24A, E71A, and E96A/E99A mutants also exhibited significant defects to virus multiplication that could not be attributed to VPg uridylylation. Substantial (10-fold) reductions in VPg uridylylation *in vitro* did not correlate directly with reductions in genome replication (e.g. compare VPg uridylylation to RNA synthesis in Table 3 for the E45A and E96A/E99A mutants). This observation is consistent with our previous study that concluded VPg uridylylation does not limit the rate of PV genome replication in tissue culture and that VPg-pUpU may be produced in vast excess of that needed for PV genome replication (14). Most of the residues of 3C implicated in VPg uridylylation by this study are located on a single convex surface of the 3C dimer (Fig. 9D). However, Glu-96 and Asp-99 are at remote sites in a dynamic region of the protein. These residues clearly use an indirect mechanism, perhaps molecular dynamics, to alter the stability of the 3C₂-3Dpol complex. Consistent with this surface interacting with 3Dpol, both the E45A and E96A/E99A mutants exhibited a synthetically lethal defect to genome replication when combined with a mutation encoding the 3Dpol-R455A derivative (Fig. 8). This and related derivatives have been shown by us to be inefficiently recruited to and/or retained in the 3C₂-oriL complex, presumably because of a suboptimal interaction of 3Dpol with the 3C dimer (data not shown and see Ref. 14).

Structural Model for the 3C₂-3Dpol Complex—We employed a molecular docking algorithm to obtain candidate models for the 3C₂-3Dpol complex. We were able to identify only one solution that was consistent with all of our current and previous molecular genetic and biochemical data (Fig. 9) (13, 14, 41). An important aspect of this model is that 3Dpol should be able to add to a 3C₂-oriL complex because a hole sufficient to accom-

moderate single-stranded RNA is visible in the 3C₂-3Dpol complex (Fig. 9B). Alignments of picornaviral 3C and 3Dpol proteins⁹ suggest that interactions between 3C₂ and 3Dpol predicted by the model (Table 4) are well conserved across the entire virus family. Residues of 3Dpol known to be involved in VPg uridylylation (e.g. 406, 455, and 461) map to the interface (Fig. 9D) (14, 41).⁸ Kirkegaard and co-workers (42) performed charged-to-alanine-scanning mutagenesis of 3Dpol. This study was the first to suggest a role for residues 455 and 456 in some aspect of genome replication (42). That study also identified many other residues that were required for genome replication that remain to be characterized. Many of these map on or very near the surface of 3Dpol proposed to interact with 3C₂ (Fig. 10A). Importantly, some of these mutants rendered virus multiplication temperature-sensitive, perhaps representing the first PV mutants that are temperature-sensitive for VPg uridylylation. DeRisi and co-workers (35) recently reported unexpected levels of diversity in 3C- and 3Dpol-coding sequence for human rhinoviruses. The only other region of the genome with a similar density of diversity is capsid-coding sequence, which is clearly under pressure to escape the humoral immune response. Interestingly, many of the residues in 3Dpol (Fig. 10B, panel i) and 3C (Fig. 10B, panel ii) under purifying selective pressure map on or very near the 3C₂-3Dpol interface. It is possible that the overlap between pre-replication and VPg uridylylation functions of 3CD reported here is driving the rapid evolution of these regions of the genome. Together, these data add validity to our structural model, moving studies of picornavirus VPg uridylylation into the structural era.

Acknowledgments—We thank Professor Coray Colina for helpful discussions regarding construction and evaluation of the structural model for 3C₂-3Dpol. We thank Hyung Suk Oh for assistance with infectious center and luciferase assays.

REFERENCES

- Racaniello, V. R. (2001) in *Fields Virology* (Knipe, D. M., Howley, P. M., Griffin, D. E., Lamb, R. A., Martin, M. A., Roizman, B., and Straus, S. E., eds) 4th Ed., pp. 685–722, Lippincott-Raven Publishers, Philadelphia
- Semler, B. L., and Wimmer, E. (eds) (2002) *Molecular Biology of Picornaviruses*, American Society for Microbiology, Washington, D. C.
- Paul, A. V. (2002) in *Molecular Biology of Picornaviruses* (Semler, B. L., and Wimmer, E., eds) 1st Ed., pp. 227–246, American Society for Microbiology, Washington, D. C.
- Paul, A. V., van Boom, J. H., Filippov, D., and Wimmer, E. (1998) *Nature* **393**, 280–284
- Paul, A. V., Rieder, E., Kim, D. W., van Boom, J. H., and Wimmer, E. (2000) *J. Virol.* **74**, 10359–10370
- Rieder, E., Paul, A. V., Kim, D. W., van Boom, J. H., and Wimmer, E. (2000) *J. Virol.* **74**, 10371–10380
- Goodfellow, I., Chaudhry, Y., Richardson, A., Meredith, J., Almond, J. W., Barclay, W., and Evans, D. J. (2000) *J. Virol.* **74**, 4590–4600
- Morasco, B. J., Sharma, N., Parilla, J., and Flanagan, J. B. (2003) *J. Virol.* **77**, 5136–5144
- Murray, K. E., and Barton, D. J. (2003) *J. Virol.* **77**, 4739–4750
- van Ooij, M. J., Vogt, D. A., Paul, A., Castro, C., Kuijpers, J., van Kuppeveld, F. J., Cameron, C. E., Wimmer, E., Andino, R., and Melchers, W. J. (2006) *J. Gen. Virol.* **87**, 103–113
- Gerber, K., Wimmer, E., and Paul, A. V. (2001) *J. Virol.* **75**, 10979–10990
- Nayak, A., Goodfellow, I. G., and Belsham, G. J. (2005) *J. Virol.* **79**, 7698–7706
- Pathak, H. B., Arnold, J. J., Wiegand, P. N., Hargittai, M. R., and Cameron, C. E. (2007) *J. Biol. Chem.* **282**, 16202–16213
- Shen, M., Wang, Q., Yang, Y., Pathak, H. B., Arnold, J. J., Castro, C., Lemon, S. M., and Cameron, C. E. (2007) *J. Virol.* **81**, 12485–12495
- Harris, K. S., Reddigari, S. R., Nicklin, M. J., Hammerle, T., and Wimmer, E. (1992) *J. Virol.* **66**, 7481–7489
- Marcotte, L. L., Wass, A. B., Gohara, D. W., Pathak, H. B., Arnold, J. J., Filman, D. J., Cameron, C. E., and Hogle, J. M. (2007) *J. Virol.* **81**, 3583–3596
- Andino, R., Rieckhof, G. E., Achacoso, P. L., and Baltimore, D. (1993) *EMBO J.* **12**, 3587–3598
- Bergmann, E. M., Mosimann, S. C., Chernia, M. M., Malcolm, B. A., and James, M. N. (1997) *J. Virol.* **71**, 2436–2448
- Blair, W. S., Nguyen, J. H., Parsley, T. B., and Semler, B. L. (1996) *Virology* **218**, 1–13
- Blair, W. S., Parsley, T. B., Bogerd, H. P., Towner, J. S., Semler, B. L., and Cullen, B. R. (1998) *RNA (N. Y.)* **4**, 215–225
- Garnik, A. V., and Andino, R. (2000) *J. Virol.* **74**, 2219–2226
- Hammerle, T., Molla, A., and Wimmer, E. (1992) *J. Virol.* **66**, 6028–6034
- Harris, K. S., Xiang, W., Alexander, L., Lane, W. S., Paul, A. V., and Wimmer, E. (1994) *J. Biol. Chem.* **269**, 27004–27014
- Kusov, Y. Y., and Gauss-Muller, V. (1997) *RNA (N. Y.)* **3**, 291–302
- Leong, L. E., Walker, P. A., and Porter, A. G. (1993) *J. Biol. Chem.* **268**, 25735–25739
- Ohlenschläger, O., Wöhnert, J., Bucci, E., Seitz, S., Hafner, S., Ramachandran, R., Zell, R., and Gölach, M. (2004) *Structure (Lond.)* **12**, 237–248
- Parsley, T. B., Towner, J. S., Blyn, L. B., Ehrenfeld, E., and Semler, B. L. (1997) *RNA (N. Y.)* **3**, 1124–1134
- Peters, H., Kusov, Y. Y., Meyer, S., Benie, A. J., Bauml, E., Wolff, M., Rademacher, C., Peters, T., and Gauss-Muller, V. (2005) *Biochem. J.* **385**, 363–370
- Shih, S. R., Chiang, C., Chen, T. C., Wu, C. N., Hsu, J. T., Lee, J. C., Hwang, M. J., Li, M. L., Chen, G. W., and Ho, M. S. (2004) *J. Biomed. Sci.* **11**, 239–248
- Walker, P. A., Leong, L. E., and Porter, A. G. (1995) *J. Biol. Chem.* **270**, 14510–14516
- Xiang, W., Harris, K. S., Alexander, L., and Wimmer, E. (1995) *J. Virol.* **69**, 3658–3667
- Yang, Y., Rijnbrand, R., Watowich, S., and Lemon, S. M. (2004) *J. Biol. Chem.* **279**, 12659–12667
- Yin, J., Paul, A. V., Wimmer, E., and Rieder, E. (2003) *J. Virol.* **77**, 5152–5166
- Zell, R., Sidigi, K., Bucci, E., Stelzner, A., and Gölach, M. (2002) *RNA (N. Y.)* **8**, 188–201
- Kistler, A. L., Webster, D. R., Rouskin, S., Magrini, V., Credle, J. J., Schnurr, D. P., Boushey, H. A., Mardis, E. R., Li, H., and DeRisi, J. L. (2007) *Virol. J.* **4**, 40
- Thivyanathan, V., Yang, Y., Kaluarachchi, K., Rijnbrand, R., Gorenstein, D. G., and Lemon, S. M. (2004) *Proc. Natl. Acad. Sci. U. S. A.* **101**, 12688–12693
- Ferrer-Orta, C., Arias, A., Agudo, R., Perez-Luque, R., Escarmis, C., Domingo, E., and Verdager, N. (2006) *EMBO J.* **25**, 880–888
- Pathak, H. B. (2006) *Towards a Unified Model of the Initiation of the First Step of Picornavirus Genome Replication*, Ph.D. thesis, Pennsylvania State University, University Park, PA
- Tellez, A. B., Crowder, S., Spagnolo, J. F., Thompson, A. A., Peersen, O. B., Brutlag, D. L., and Kirkegaard, K. (2006) *J. Mol. Biol.* **357**, 665–675
- Paul, A. V., Yin, J., Mugavero, J., Rieder, E., Liu, Y., and Wimmer, E. (2003) *J. Biol. Chem.* **278**, 43951–43960
- Pathak, H. B., Ghosh, S. K., Roberts, A. W., Sharma, S. D., Yoder, J. D., Arnold, J. J., Gohara, D. W., Barton, D. J., Paul, A. V., and Cameron, C. E. (2002) *J. Biol. Chem.* **277**, 31551–31562
- Diamond, S. E., and Kirkegaard, K. (1994) *J. Virol.* **68**, 863–876
- Dmitrieva, T. M., Alexeevski, A. V., Shatskaya, G. S., Tolskaya, E. A., Gmyl, A. P., Khitrina, E. V., and Agol, V. I. (2007) *Virology* **365**, 79–91

⁹ A. C. Palmenberg, personal communication.

44. Herold, J., and Andino, R. (2000) *J. Virol.* **74**, 6394–6400
45. Gohara, D. W., Crotty, S., Arnold, J. J., Yoder, J. D., Andino, R., and Cameron, C. E. (2000) *J. Biol. Chem.* **275**, 25523–25532
46. Caliguri, L. A., and Tamm, I. (1968) *Virology* **35**, 408–417
47. Noble, J., and Levintow, L. (1970) *Virology* **40**, 634–642
48. Tershak, D. R. (1982) *J. Virol.* **41**, 313–318
49. Barton, D. J., Morasco, B. J., and Flanagan, J. B. (1996) *Methods Enzymol.* **275**, 35–57
50. Lyons, T., Murray, K. E., Roberts, A. W., and Barton, D. J. (2001) *J. Virol.* **75**, 10696–10708
51. Gohara, D. W., Ha, C. S., Kumar, S., Ghosh, B., Arnold, J. J., Wisniewski, T. J., and Cameron, C. E. (1999) *Protein Expression Purif.* **17**, 128–138
52. Jones, T. A., Zou, J. Y., Cowan, S. W., and Kjeldgaard, M. (1991) *Acta Crystallogr. Sect. A* **47**, 110–119
53. Phillips, J. C., Braun, R., Wang, W., Gumbart, J., Tajkhorshid, E., Villa, E., Chipot, C., Skeel, R. D., Kale, L., and Schulten, K. (2005) *J. Comput. Chem.* **26**, 1781–1802
54. Humphrey, W., Dalke, A., and Schulten, K. (1996) *J. Mol. Graphics* **14**, 33–38
55. Hansen, J. L., Long, A. M., and Schultz, S. C. (1997) *Structure (Lond.)* **5**, 1109–1122
56. Hobson, S. D., Rosenblum, E. S., Richards, O. C., Richmond, K., Kirkegaard, K., and Schultz, S. C. (2001) *EMBO J.* **20**, 1153–1163
57. Lyle, J. M., Bullitt, E., Bienz, K., and Kirkegaard, K. (2002) *Science* **296**, 2218–2222
58. Pata, J. D., Schultz, S. C., and Kirkegaard, K. (1995) *RNA (N. Y.)* **1**, 466–477
59. Mosimann, S. C., Cherney, M. M., Sia, S., Plotch, S., and James, M. N. (1997) *J. Mol. Biol.* **273**, 1032–1047
60. Belov, G. A., Altan-Bonnet, N., Kovtunovych, G., Jackson, C. L., Lippincott-Schwartz, J., and Ehrenfeld, E. (2007) *J. Virol.* **81**, 558–567
61. Belov, G. A., and Ehrenfeld, E. (2007) *Cell Cycle* **6**, 36–38
62. Belov, G. A., Fogg, M. H., and Ehrenfeld, E. (2005) *J. Virol.* **79**, 7207–7216
63. Belov, G. A., Habbersett, C., Franko, D., and Ehrenfeld, E. (2007) *J. Virol.* **81**, 9259–9267
64. Franco, D., Pathak, H. B., Cameron, C. E., Rombaut, B., Wimmer, E., and Paul, A. V. (2005) *J. Virol.* **79**, 6358–6367
65. Franco, D., Pathak, H. B., Cameron, C. E., Rombaut, B., Wimmer, E., and Paul, A. V. (2005) *Virol. J.* **2**, 86
66. Wimmer, E., Hellen, C. U., and Cao, X. (1993) *Annu. Rev. Genet.* **27**, 353–436
67. Thompson, A. A., and Peersen, O. B. (2004) *EMBO J.* **23**, 3462–3471
68. Tovchigrechko, A., and Vakser, I. A. (2006) *Nucleic Acids Res.* **34**, W310–W314
69. Maynell, L. A., Kirkegaard, K., and Klymkowsky, M. W. (1992) *J. Virol.* **66**, 1985–1994
70. Hammerle, T., Hellen, C. U., and Wimmer, E. (1991) *J. Biol. Chem.* **266**, 5412–5416
71. Cuconati, A., Molla, A., and Wimmer, E. (1998) *J. Virol.* **72**, 6456–6464
72. Doedens, J., Maynell, L. A., Klymkowsky, M. W., and Kirkegaard, K. (1994) *Arch. Virol.* **9**, S159–S172

**Picornavirus Genome Replication: IDENTIFICATION OF THE SURFACE OF
THE POLIOVIRUS (PV) 3C DIMER THAT INTERACTS WITH PV 3Dpol
DURING VPg URIDYLYLATION AND CONSTRUCTION OF A
STRUCTURAL MODEL FOR THE PV 3C2-3Dpol COMPLEX**

Miaoqing Shen, Zachary J. Reitman, Yan Zhao, Ibrahim Moustafa, Qixin Wang, Jamie
J. Arnold, Harsh B. Pathak and Craig E. Cameron

J. Biol. Chem. 2008, 283:875-888.

doi: 10.1074/jbc.M707907200 originally published online November 9, 2007

Access the most updated version of this article at doi: [10.1074/jbc.M707907200](https://doi.org/10.1074/jbc.M707907200)

Alerts:

- [When this article is cited](#)
- [When a correction for this article is posted](#)

[Click here](#) to choose from all of JBC's e-mail alerts

This article cites 68 references, 39 of which can be accessed free at
<http://www.jbc.org/content/283/2/875.full.html#ref-list-1>